

## THE X-RAY PROPERTIES OF LOW-FREQUENCY QUASI-PERIODIC OSCILLATIONS FROM GRS 1915+105 UP TO 120 KEV

JOHN A. TOMSICK

Center for Astrophysics and Space Sciences, University of California, San Diego, MS 0424, La Jolla, CA 92093 (e-mail: jtomsick@ucsd.edu)

PHILIP KAARET

Harvard-Smithsonian Center for Astrophysics, 60 Garden Street, Cambridge, MA 02138 (e-mail: pkaaret@cfa.harvard.edu)

*To Appear in the Astrophysical Journal*

### ABSTRACT

We present a study of the properties of strong 0.8-3.0 Hz quasi-periodic oscillations (QPOs) that occurred during 1997 *Rossi X-ray Timing Explorer* (*RXTE*) observations of the microquasar GRS 1915+105 in the low-hard state. The high count rates allow us to track individual QPO peaks, and we exploit this to develop a QPO folding technique. In contrast to previous QPO studies with *RXTE*, we emphasize the high energy QPO properties and report the detection of a QPO in the 60-124 keV energy band. Our technique allows us, for the first time, to measure the phase of the QPO harmonics relative to the fundamental. Variation in this phase difference leads to changes in the shape of the QPO profile with energy and over time. The strength of the QPO fundamental increases up to 19 keV, but the data do not suggest that the strength continues to increase above this energy. In some cases, the QPO amplitudes in the 30-60 keV and 60-124 keV energy bands are significantly less than in the 13-19 keV and 19-29 keV energy bands. We also use our technique to measure the phase lag of the QPO fundamental and harmonics. In the case where negative phase lags are detected for the fundamental, positive phase lags are detected for the first harmonic.

*Subject headings:* accretion, accretion disks — X-ray transients: general — stars: individual (GRS 1915+105)  
— stars: black holes — X-rays: stars

### 1. INTRODUCTION

The *Rossi X-ray Timing Explorer* (Bradt, Rothschild & Swank 1993) has provided an unprecedented opportunity to study the timing properties of X-ray binaries. *RXTE* observations of black hole candidates (BHCs) indicate that modulations in the X-ray flux (i.e., quasi-periodic oscillations or QPOs) occur on time scales from milliseconds to hundreds of seconds. In this paper, we focus on QPOs from one of the most studied *RXTE* targets, GRS 1915+105. This BHC X-ray transient and microquasar (Mirabel & Rodriguez 1994) has the richest variety of timing behavior of any X-ray binary observed to date (e.g., Greiner, Morgan & Remillard 1996; Belloni et al. 2000).

Previous studies of GRS 1915+105 show that the QPO properties are closely related to the properties of the energy spectrum. In these studies, the energy spectrum was modeled using a two component model consisting of a soft component, which presumably comes from an optically thick accretion disk, and a hard component, which is thought to be due to inverse Comptonization of soft photons from the accretion disk. Markwardt et al. (1999) and Munro et al. (1999) find that the QPO frequency is closely related to the properties of the soft component and, thus, the accretion disk. It has also been found that the strength of the QPO increases with energy up to at least 15 keV, indicating that the QPO mechanism modulates the hard component (e.g., Morgan, Remillard & Greiner 1997). If the hard component is produced via inverse Comptonization, a hard phase lag is expected. While hard phase lags have been observed for several sources, Reig et al. (2000) find soft phase lags for GRS 1915+105 in some cases, and, in this paper, we include some of the observations where soft phase lags were observed.

We present a detailed study of 0.8-3.0 Hz QPOs that occurred

during 1997 October *RXTE* observations. The high Proportional Counter Array (PCA) count rates allow us to track individual QPO peaks, and we have exploited this to develop a QPO folding technique with some similarities to that used by Morgan et al. (1997). In contrast to previous QPO studies with *RXTE*, we emphasize the high energy QPO properties and report the detection of a QPO in the 60-124 keV band using the High Energy X-ray Timing Experiment (HEXTE). Here, we study how the properties of the QPO fundamental and first and second harmonics change with energy and between observations. We measure the phase of the QPO harmonics relative to the fundamental and the strength and phase of the fundamental and harmonics over the full *RXTE* band-pass.

### 2. OBSERVATIONS

We chose the 1997 October *RXTE* observations from the large number of GRS 1915+105 observations between the start of the *RXTE* mission and early 1998 based on our goal of extending QPO measurements to high energies. We searched the public archive for observations with strong low-frequency QPOs and a high HEXTE count rate, and found that observations during low-hard states (Morgan et al. 1997) provide the best match to these criteria. Between the start of the *RXTE* mission and early 1998 the low-hard state occurred three times for GRS 1915+105 as shown in Figure 9 of Belloni et al. (2000) along with the *RXTE* All-Sky Monitor (ASM) light curve<sup>1</sup> In the 1.5-12 keV ASM light curve, the low-hard states appear as low flux time periods with very little variability. Ultimately, we chose to focus on the third low-hard state. This decision was made because HEXTE was not rocking during the first low-

<sup>1</sup>Note that Belloni et al. (2000) refer to the low-hard state as class  $\chi$ .

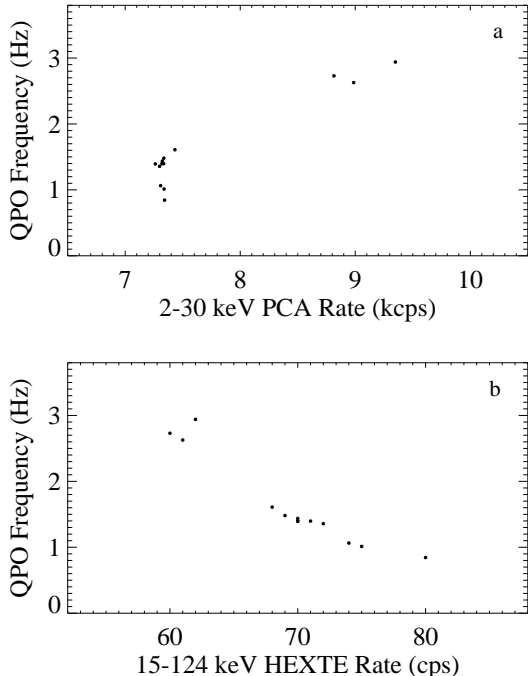


FIG. 1.— QPO frequency vs. count rate for (a) the PCA in the 2-30 keV band and (b) HEXTE in the 15-124 keV band. The numbers used to generate these plots are given in Table 1.

hard state, making background subtraction with standard techniques impossible, and because the QPO frequency is lower for the third low-hard state than for the second low-hard state (Trudolyubov, Churazov & Gilfanov 1998; Reig et al. 2000). Since our folding technique depends on being able to detect individual QPO peaks, low frequency QPOs provide a significant advantage.

During the third low-hard state, six *RXTE* observations were made over thirteen *RXTE* orbits. For each of the thirteen orbits, Table 1 gives the time at the midpoint of the unocculted part of the orbit, the exposure time, the QPO frequency during the orbit, which we determined by making and fitting power spectra for each orbit, the 2-30 keV PCA count rate and the 15-124 keV HEXTE count rate. The PCA count rates are between 7300 and 9500 cps, and the HEXTE count rates are between 60 and 80 cps. Figure 1 shows the QPO frequencies as a function of count rate for PCA and HEXTE. The correlation between the PCA rate and the QPO frequency is apparent and has been noticed before for this data (Reig et al. 2000). Interestingly, there is an anti-correlation between the HEXTE rate and the QPO frequency that is even more striking. The 2-30 keV PCA light curve for 15 s of orbit 4 is shown in Figure 2a, and the presence of the QPO is obvious.

### 3. ANALYSIS

For each *RXTE* orbit, we extracted the 2-30 keV PCA light curve with 7.8125 ms time resolution. We made and fitted power spectra to determine QPO frequencies (see Table 1) for each orbit. A band-pass filter with frequency limits 20% below

and above the QPO frequency was applied to the light curve, and the filtered light curve for 15 s of orbit 4 is shown in Figure 2b. We used a Kaiser band-pass filter, which is a finite impulse response filter with a Kaiser window (Jackson 1989). Derivatives of the filtered light curve were calculated to find the minima between QPO pulses. To determine which minima are significant, we simulated a light curve with a white noise power spectrum and the same statistics as the observed light curve. We applied the band-pass filter to the white noise light curve, and the result is the dashed line in Figure 2b. In the filtered version of the observed light curve, minima are defined as the places where the first derivative of the filtered light curve is zero, the second derivative of the filtered light curve is positive and the minimum is lower than 99.9% of the minima in the filtered white noise light curve.

The minima from the 2-30 keV PCA light curve are used to fold the light curves in different energy bands. We extracted PCA and HEXTE light curves in several energy bands. The standard deadtime correction is applied to the HEXTE data. To fold the light curves, we assign a pulse phase to each light curve time bin. We define the light curve minima to be at a pulse phase of  $180^\circ$  and determine phases for the other time bins by interpolating between minima. A plot of count rate vs. phase provides the folded light curve. This method allows us to combine data from orbits with slightly different QPO frequencies. Representative folded light curves for PCA and HEXTE are shown in Figure 3. After folding as described above, the light curve is rebinned in phase. Poisson error bars are shown and

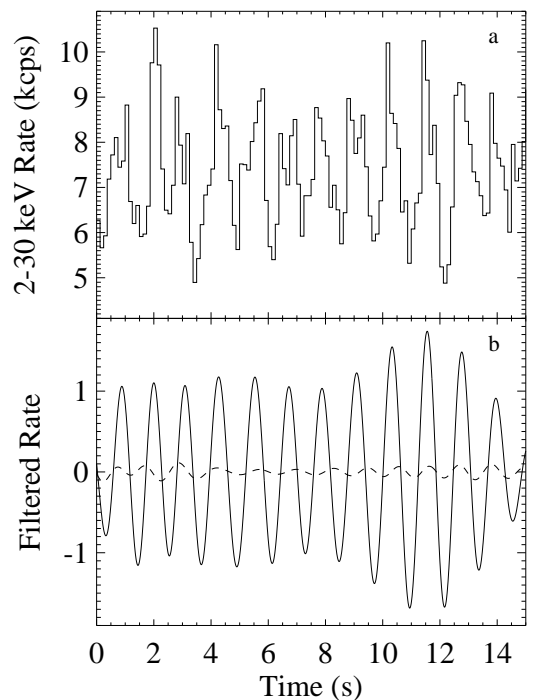


FIG. 2.— (a) The 2-30 keV PCA light curve for 15 s of orbit 4 with a time resolution of 0.125 s. (b) The same light curve after band-pass filtering (solid line). For comparison, the dashed line shows a white noise light curve after band-pass filtering.

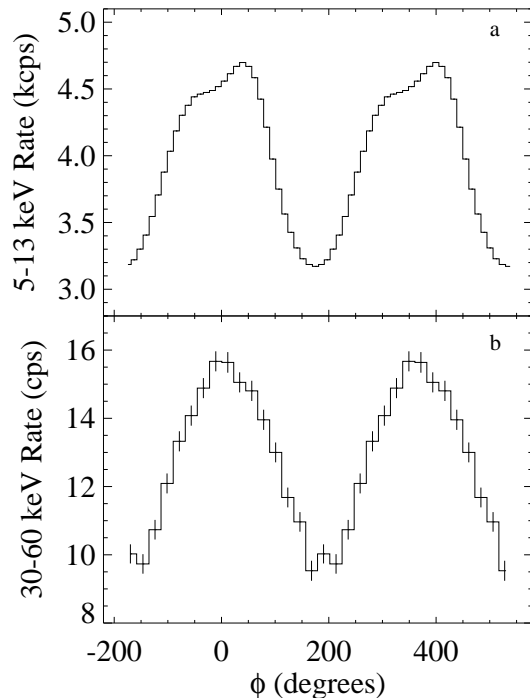


FIG. 3.— Folded (a) PCA and (b) HEXTE light curves for the combination of orbits 7-13. The 5-13 keV PCA and the 30-60 keV HEXTE energy bands are shown, and two QPO cycles are displayed.

two cycles are displayed.

To optimize and test our software, we applied our folding technique to simulated light curves. We used the GRS 1915+105 power spectra to determine the properties of the simulated light curves. We made and fitted power spectra for each of the thirteen orbits, and we refer the reader to Reig et al. (2000) for figures showing a representative sample of these. The power spectra contain a low-frequency (0.8-3.0 Hz) QPO with a fractional rms amplitude of about 10% and its first harmonic with an rms amplitude near 5%. Our simulated light curves contain a sinusoidal modulation with a frequency of 1 Hz and an amplitude of 14% of the mean level, which corresponds to an rms amplitude of 10%. A harmonic is included by adding a second sinusoid with twice the frequency and half the strength of the first sinusoid. A fixed but arbitrary phase difference between the two sinusoids is assumed. The signal is made to be quasi-periodic by stretching or compressing each cycle (i.e., pulse) in time. Although the pulse profile remains constant throughout, the pulse duration changes for each cycle. Motivated by the results of Morgan et al. (1997), who found that the phase of the QPO relative to a periodic signal performs a random walk over time, we vary the pulse duration so that it performs a random walk from pulse-to-pulse. Since a changing pulse duration leads to a corresponding change in the phase of the QPO, we set the step size for the random walk to reproduce the magnitude of the phase changes observed for GRS 1915+105 by Morgan et al. (1997). Finally, we checked that our simulated light curves have properties consistent with those of the actual GRS 1915+105 light curves by making power spectra for the

simulated light curves. The power spectra contain a QPO and its harmonic, and the widths of these features are consistent with those found for the actual GRS 1915+105 power spectra.

We applied our QPO folding technique, which is outlined above, to the simulated light curves. Figure 4 shows the result for a representative simulated light curve. In this example, the largest discrepancy between the folded light curve and the input profile for any phase bin is 0.7% of the mean count rate. For optimization of our technique, we filtered the simulated light curves using several different frequency limits for the band-pass. As long as the band-pass is wide enough to contain the random-walking QPO frequency, the results do not depend sensitively on the exact frequency limits used for the filter, and frequency limits 20% below and above the QPO frequency provided a band-pass wide enough for GRS 1915+105. We applied a band-pass filter with these frequency limits to 100 simulated light curves, and, for each light curve, we determined the largest discrepancy between the folded light curve and the input profile. On average, the largest discrepancy was 0.74% of the mean count rate, and, for 95 of the 100 simulated light curves, the largest discrepancies were less than 1%. We produced simulated light curves with various phase differences between the QPO and its harmonic. Although the shape of the QPO profile changes, the discrepancies between the folded light curve and the input profile do not change significantly.

Using our technique for finding the minima in the GRS 1915+105 light curve, 95% to 99% of the expected minima are detected. This either indicates that there are irregularities in the light curve (e.g., the QPO turns off for a small fraction of the time) or that our technique is not sensitive enough to detect a small fraction of the minima. In order to determine where minima are being missed, we calculated the ratio of the time to the previous minimum to the time to the next minimum for each detected minimum. The ratio is close to 1.0 in cases where there are

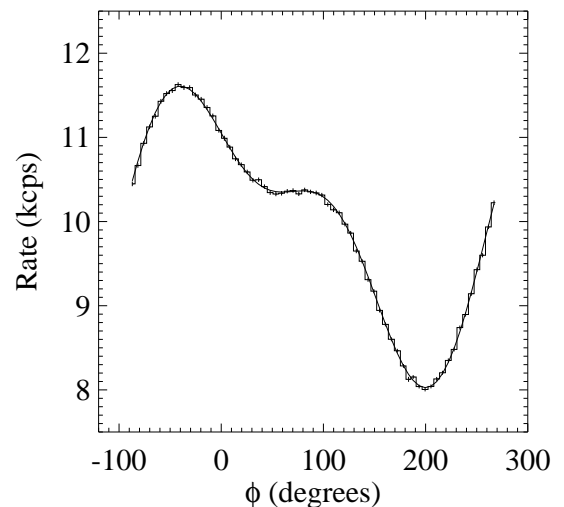


FIG. 4.— Comparison between a folded light curve and the input QPO profile for the simulation. The largest discrepancy between the folded light curve and the input profile for any phase bin is 0.74% of the mean count rate.

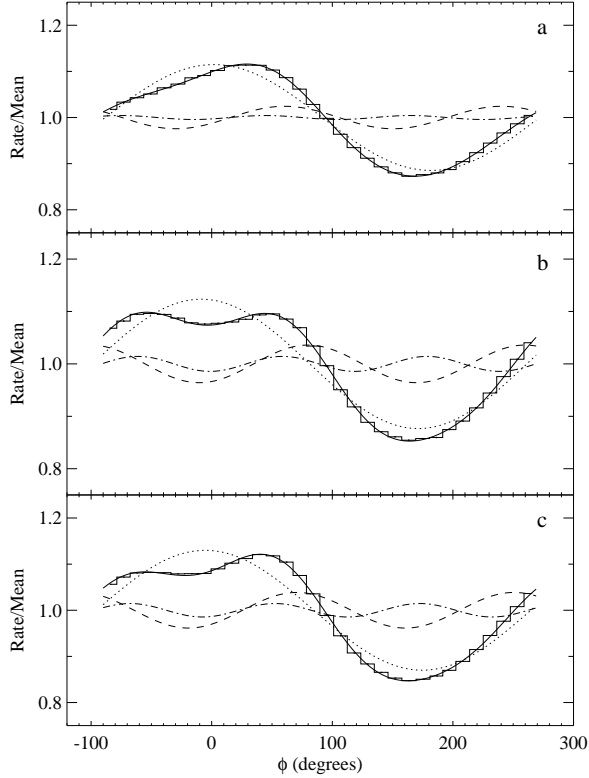


FIG. 5.— The 2-5 keV folded light curves (Rate/Mean) vs. phase for orbits 1-3 (a), 4-6 (b) and 7-13 (c). The solid line is a fit to the light curve with a model consisting of a constant and three harmonically spaced sinusoids (see Equation 1). The fundamental (dotted line), first harmonic (dashed line) and second harmonic (dot-dashed line) are also shown separately.

no missing minima, but significantly deviates from 1.0 where missing minima occur. To avoid including data with indeterminate phases, we rejected data surrounding missing minima. In the worst case, this technique led to rejecting 8% of the data, and, for most orbits, between 2% and 4% of the data were rejected.

#### 4. RESULTS

We produced folded light curves in five PCA energy bands (2-5 keV, 5-13 keV, 13-19 keV, 19-29 keV and 29-60 keV) and four HEXTE energy bands (16-18 keV, 18-30 keV, 30-60 keV and 60-124 keV) for each of the thirteen *RXTE* orbits. We examined the folded light curves and found that the shape of the folded light curve changes during the thirteen orbits. However, in some cases, the shape is very similar for consecutive orbits, and, in these cases, we combined the data from multiple orbits. The longest stretch of time during which the shape remains stable is more than 3 d during orbits 7-13. Also, the QPO profile can change significantly on time scales less than 5 or 6 d. We characterize the folded light curves by fitting them with harmonically related sinusoids. From Figure 3, it is clear that one sinusoid does not provide a good description of the folded light curves, especially at low energy. Adding more sinusoids improves the fits considerably, and three sinusoids provide a good description of the data. We note that the presence of a QPO

with two harmonics is consistent with the power spectra shown by Reig et al. (2000). We fitted the folded light curves with the function

$$f(\phi) = a_0 + a_1 \sin(\phi - \phi_1) + a_2 \sin[2(\phi - \phi_2)] + a_3 \sin[3(\phi - \phi_3)] \quad (1)$$

and, below, we refer to  $\phi_i$  as the phase of the sinusoid, and we define the amplitudes of the sinusoids as  $A_i = a_i/a_0$ , where  $i$  runs from 1 to 4. For most energy bands, the phase-averaged deviations between this model and the folded light curve are less than 1%. The deviations are somewhat larger in a few cases where the folded light curves have relatively low statistics. In these cases, low reduced chi-squared values ( $\chi^2/\nu < 0.8$  for 25 degrees of freedom for the PCA and  $\chi^2/\nu < 1.3$  for 9 degrees of freedom for HEXTE) indicate that the model provides a good description of the data.

In Figure 5, we show the 2-5 keV folded light curves for orbits 1-3, 4-6 and 7-13, fitted with the model described above. The solid line shows the combination of three sinusoids, and the fundamental (dotted line), first harmonic (dashed line) and second harmonic (dot-dashed line) are also shown. While the commonly used power spectrum does not provide information about the phase difference between sinusoidal components, our folding technique does provide this information. Phase information can be derived from examination of the full complex

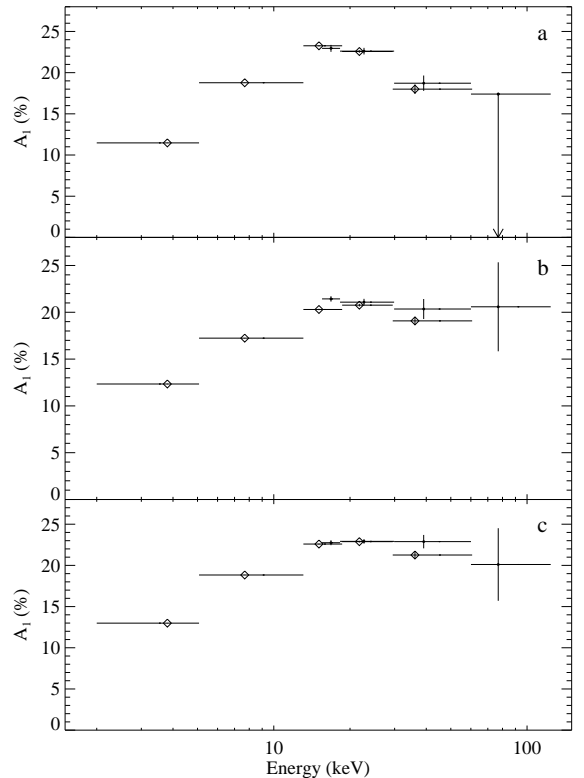


FIG. 6.— The QPO amplitude of the fundamental ( $A_1$ ) vs. energy for orbits 1-3 (a), 4-6 (b) and 7-13 (c). The diamonds mark PCA measurements and the points mark HEXTE measurements. The error bars shown correspond to 68% confidence, and the 95% confidence upper limit is shown for the 60-124 keV energy band in panel a.

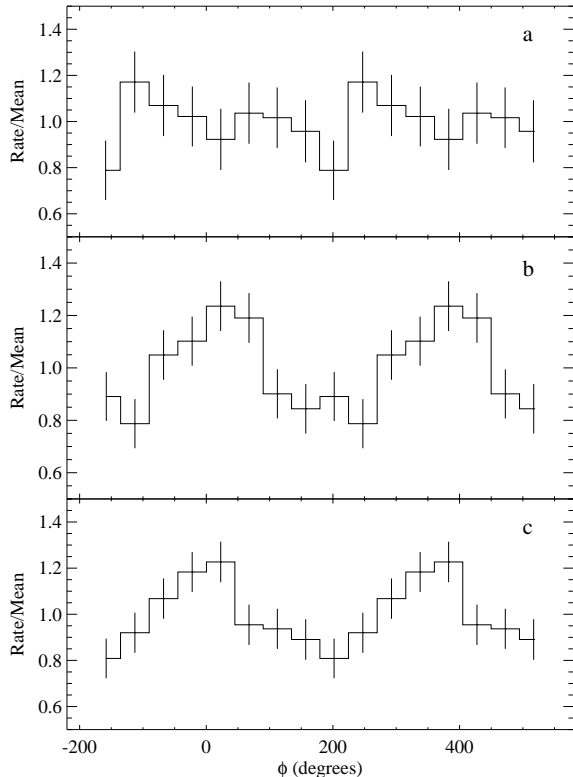


FIG. 7.— The 60-124 keV folded light curves (Rate/Mean) vs. phase for orbits 1-3 (a), 4-6 (b) and 7-13 (c) using HEXTE. Two QPO cycles are displayed. QPOs are detected for orbits 4-6 and 7-13, but not for orbits 1-3. The 95% confidence upper limit on the QPO amplitude for orbits 1-3 is 17.4%.

Fourier transform, but this is only rarely accomplished and has not been done in analyses of GRS 1915+105. Table 2 gives the values of  $\phi_1 - \phi_2$ ,  $\phi_1 - \phi_3$  and  $\phi_2 - \phi_3$  for the 2-5 keV folded light curves. The shape of the folded light curve depends on the phase difference between the sinusoidal components. The largest change in the shape of the folded light curve occurs because of changes in the phase difference between the fundamental and the two harmonics. The variation in  $\phi_2 - \phi_3$  over time is smaller. In addition, we note that the double peaking observed for orbits 4-6 occurs because the minima of the harmonics occur at nearly the same phase as the maximum of the fundamental.

Figure 6 shows the amplitudes of the fundamental ( $A_1$ ) for energies from 2 to 124 keV for orbits 1-3, 4-6 and 7-13 using PCA and HEXTE. In the region where PCA and HEXTE overlap, there is good agreement between the two instruments. In all cases,  $A_1$  increases with energy up to 19 keV, changing from between 11% and 13% in the lowest energy band up to between 20% and 24% in the 13-19 keV energy band, but the data do not suggest that  $A_1$  continues to increase above 19 keV. While there is strong evidence for a drop in  $A_1$  at higher energies for orbits 1-3, the data do not require a decrease in  $A_1$  above 19 keV for orbits 4-6 and 7-13. However, for orbits 4-6 and 7-13, it should be noted that  $A_1$  does not increase with energy at the same rate above 19 keV as it does between 2 keV and 19 keV. Figure 7 shows the 60-124 keV folded light curves for the three

cases. While the QPO is detected at high confidence for orbits 4-6 and 7-13, the QPO is not detected for orbits 1-3, and we derive a 95% confidence upper limit ( $\Delta\chi^2 = 4$ ) of 17.4% on  $A_1$ . The upper limit is found using the model with three harmonic components described above and leaving the fit parameters free while stepping through values of  $a_1$ . The results indicate that  $A_1$  is significantly lower for energy bands 30-60 keV and 60-124 keV than for 13-19 keV and 19-29 keV. Figure 8 shows the amplitudes of the first harmonic ( $A_2$ ) vs. energy. For orbits 4-6 and 7-13,  $A_2$  is between 3.5% and 4.0% at low energies and decreases at higher energies. For orbits 1-3,  $A_2$  drops at intermediate energies but may increase again above 30 keV. Figure 9 shows the amplitudes of the second harmonic ( $A_3$ ) vs. energy. The increase in  $A_3$  at low energies provides some evidence for similar behavior for the second harmonic and the fundamental. In addition, like  $A_1$ ,  $A_3$  appears to level off or decrease at higher energies. For orbits 7-13, the data strongly suggests that  $A_3$  peaks around 10 keV and decreases at high energies. Values of  $A_2$  and  $A_3$  are not well-constrained for the 60-124 keV energy band and are not shown.

Figure 10 shows the phase lag of the fundamental ( $\Delta\phi_1$ ) for different energies up to 60 keV relative to the 2-5 keV energy band (i.e.,  $\Delta\phi_1 = \phi_1(E) - \phi_1(2-5 \text{ keV})$ ) for orbits 1-3, 4-6 and 7-13 using PCA and HEXTE. As we found for the amplitude, the PCA and HEXTE measurements are consistent. The values of  $\Delta\phi_1$  we find for the 5-13 keV energy band are consistent with the phase lag values found by Reig et al. (2000) using

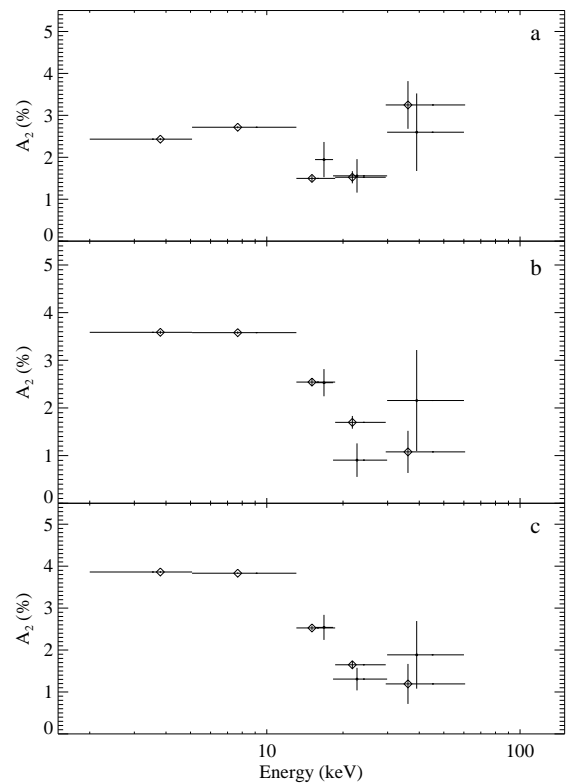


FIG. 8.— The QPO amplitude of the first harmonic ( $A_2$ ) vs. energy for orbits 1-3 (a), 4-6 (b) and 7-13 (c). The diamonds mark PCA measurements and the points mark HEXTE measurements.

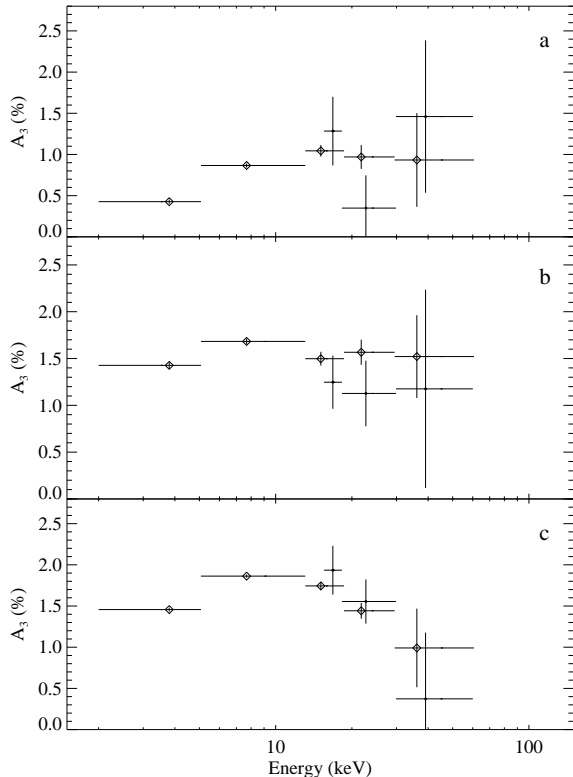


FIG. 9.— The QPO amplitude of the second harmonic ( $A_3$ ) vs. energy for orbits 1-3 (a), 4-6 (b) and 7-13 (c). The diamonds mark PCA measurements and the points mark HEXTE measurements.

cross-spectral techniques. For orbits 1-3, our results show that the negative phase lags reported by Reig et al. (2000) for the 5-13 keV energy band become more negative at higher energies. For orbits 4-6 and 7-13, the phase lags are positive and increase steadily with energy. Figure 11 shows the phase lag of the first harmonic ( $\Delta\phi_2$ ) relative to the 2-5 keV energy band. For orbits 1-3, positive phase lags are seen for the first harmonic above 13 keV, in contrast to the negative phase lags found for the fundamental. For orbits 4-6 and 7-13, the phase lags for the first harmonic are also positive, but they are significantly smaller than for orbits 1-3 and somewhat smaller than the phase lags found for the fundamental for orbits 4-6 and 7-13. Figure 12 shows the phase lag of the second harmonic ( $\Delta\phi_3$ ) relative to the 2-5 keV energy band. There is some evidence that the second harmonic has negative lags for orbits 1-3; however, the significance of the detection is marginal. For orbits 4-6 and 7-13, there is marginal evidence for positive lags. Note that the phase lag for the second harmonic is not well constrained by HEXTE for the 30-60 keV energy band and is not shown.

## 5. DISCUSSION

Our results for GRS 1915+105 focus on the energy dependence of the QPO amplitude and phase lags for the QPO fundamental and its first two harmonics. In this section, we discuss how our results relate to some of the proposed models to explain the X-ray timing properties of BHCs. Recent work by Lehr, Wagoner & Wilms (2000) provides one of the only de-

tailed predictions for the energy dependence of the QPO amplitude for BHCs. Assuming that the hard X-rays are produced by Comptonization in a corona with a radial temperature gradient, Lehr et al. (2000) predict that, in some cases, the QPO amplitude will decrease at high energies, similar to what we observe for GRS 1915+105. In their Monte Carlo simulations, Lehr et al. (2000) assume that the QPO is due to the flux modulation of soft seed photons which are subsequently Compton upscattered in a corona. The total X-ray flux emitted is the combination of the flux from regions where the QPO is active and the flux from other regions where the soft photons are unmodulated. In a given energy band, the predicted QPO amplitude is given by the ratio of the flux that emerges in this energy band from the region where the QPO is active to the total flux in this energy band. If the corona has a temperature gradient, and is hottest in the region where the QPO is active, then a QPO amplitude that increases with energy is predicted because the highest energy photons come from the region where the QPO is active. However, if the QPO is active in a region where the corona is cooler, then a drop in the QPO amplitude at high energies is predicted. Within this model, observing the amplitude as a function of photon energy can be used to gain insight into where the QPO originates. If it is assumed that the electron temperature decreases with distance from the compact object (e.g., if the energy deposition in the corona becomes less efficient at larger radii), then QPOs originating in the accretion disk at a greater distance from the compact object will exhibit a larger drop in amplitude at high energies.

Results for the GRS 1915+105 QPOs appear to be qualitatively consistent with the simulations of Lehr et al. (2000) if it is assumed that lower frequency QPOs originate further out in the accretion disk, which would be the case if the QPO frequency is related to the dynamical time scale where the QPO is produced. For GRS 1915+105, Cui (1999) finds that the 0.067 Hz QPO amplitude peaks between 7 keV and 10 keV. Our results show that the amplitude of the 2.6-3.0 Hz QPO (orbits 1-3) peaks between 13 keV and 30 keV. The fact that the amplitude of this QPO peaks at a higher energy than the amplitude of the 0.067 Hz QPO is consistent with a QPO production site closer to the compact object. Finally, the 67 Hz QPO observed for GRS 1915+105 is also consistent with this picture since its amplitude has only been observed to increase with energy in the PCA energy range where it is detected (Morgan et al. 1997). However, the highest energy band where the 67 Hz QPO has been detected is only 15-25 keV.

It is difficult to explain the negative phase lags observed for the QPO fundamental for orbits 1-3. If hard X-rays are produced by inverse Comptonization, then one expects the hard X-rays to be delayed relative to the soft X-rays, which results in positive phase lags as is observed for orbits 4-6 and 7-13. Reig et al. (2000) find that the phase lags for the continuum noise are also negative in some cases when the QPO phase lags are negative, and any model to explain the negative QPO phase lags should also be able to explain the negative continuum phase lags. Such a model, motivated by observations of GRS 1915+105, has been proposed by Nobili et al. (2000). Their model assumes that the optical depth of the Comptonizing region increases as the inner edge of the disk moves closer to the compact object so that Compton down-scattering (instead

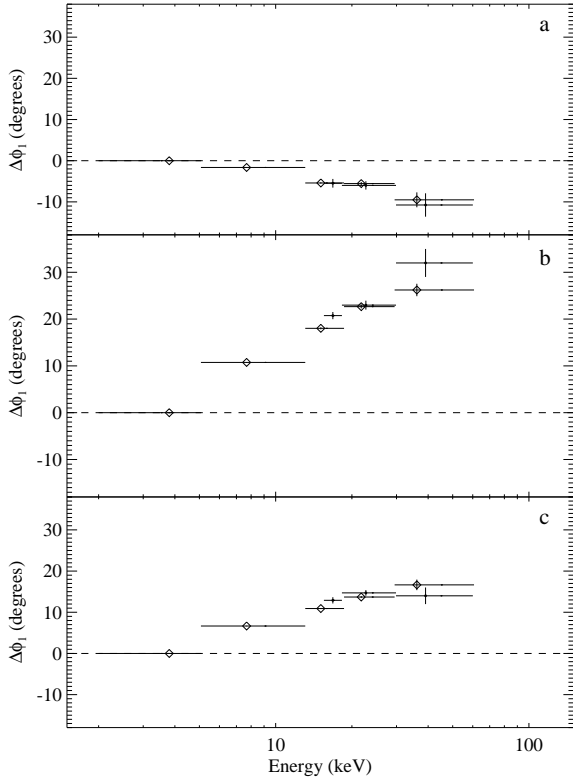


FIG. 10.— The phase lag for the fundamental vs. energy relative to the 2-5 keV energy band (i.e.,  $\Delta\phi_1 = \phi_1(E) - \phi_1(2-5 \text{ keV})$ ) for orbits 1-3 (a), 4-6 (b) and 7-13 (c). The diamonds mark PCA measurements and the points mark HEXTE measurements.

of up-scattering) dominates when the inner edge of the disk is close to the compact object. At this point, the model of Nobili et al. (2000) provides a possible explanation for the behavior of the continuum, but more work is necessary to see if the model can reproduce all the observed QPO properties.

Although the model of Nobili et al. (2000) may be able to explain the negative phase lags for the QPO fundamental, it is not clear if the model will be able to explain the simultaneous positive phase lags for the first harmonic. This phenomenon (alternating negative and positive phase lags between the QPO fundamental and its first harmonic) has also been observed for the BHC XTE J1550–564 (Wijnands, Homan & van der Klis 1999; Sobczak et al. 2000). An explanation for this behavior has been suggested by Böttcher & Liang (2000). They assume that inverse Comptonization is still the dominant process, but, in addition, they assume that the light travel time between the location where the soft photons are emitted and the Comptonization region is longer than half of the fundamental QPO period, making a hard lag appear to be a soft lag. Depending on the distance between the source of soft photons (i.e., the optically thick accretion disk) and the Comptonization region, the model can produce positive lags (i.e., apparent hard lags) or negative lags (i.e., apparent soft lags). Negative lags are predicted for higher frequencies, which is consistent with the properties of the low-frequency QPOs in GRS 1915+105. In certain cases, the model of Böttcher & Liang (2000) predicts negative

lags for the fundamental, positive lags for the first harmonic and negative lags for the second harmonic. For GRS 1915+105, we observe positive lags for the first harmonic, and, although our results suggest that the phase lags for the second harmonic may be negative, the evidence for this is marginal. While this model may provide explanations for the observed QPO phase lags, it is not clear if it can explain the negative phase lags observed for the continuum noise.

## 6. SUMMARY AND CONCLUSIONS

Our study of the broadband properties of the low-frequency QPOs in GRS 1915+105 provides several new results. We developed a QPO folding technique allowing us to study the detailed properties of the GRS 1915+105 QPOs. We successfully tested the folding technique using simulations, and, where comparison is possible, our results are consistent with previous results that relied on standard Fourier techniques. We report the first detection of QPOs with HEXTE, making it possible to measure QPO amplitudes and phase lags up to 124 keV. The highest energy band where we achieved a detection is 60-124 keV. In the energy range where there is overlap between the PCA and HEXTE, we find good agreement between the two instruments for the QPO properties. While our results confirm that the QPO amplitude increases with energy up to 19 keV, they also indicate that the QPO amplitude does not increase at the same rate above 19 keV as it does at lower energies. For orbits 1-3, the QPO amplitudes in the 30-60 keV and 60-124 keV energy bands are significantly less than in the 13-19 keV and 19-29 keV energy bands. Also, for orbits 1-3, we confirm the negative phase lag for the QPO fundamental reported by Reig et al. (2000), and we report a positive phase lag for the first harmonic. Variation in the phase difference between sinusoidal components leads to changes in the shape of the QPO profile with energy and over time. Our results show that, in some cases, the QPO profile remains unchanged for more than 3 d even as the QPO frequency varies by 17% (orbits 7-13). Also, the QPO profile can change significantly on time scales less than 5 or 6 d. Although the physical models developed by Lehr et al. (2000), Nobili et al. (2000) and Böttcher & Liang (2000) and discussed here each can explain aspects of the GRS 1915+105 timing properties, it is not clear if any of the models can reproduce all the observed timing properties. More detailed comparisons between the data and the model predictions are necessary.

JAT would like to acknowledge participants of the Rossi 2000 meeting at Goddard Space Flight Center in 2000 March for useful discussions and Jörn Wilms for comments on a draft of this paper.

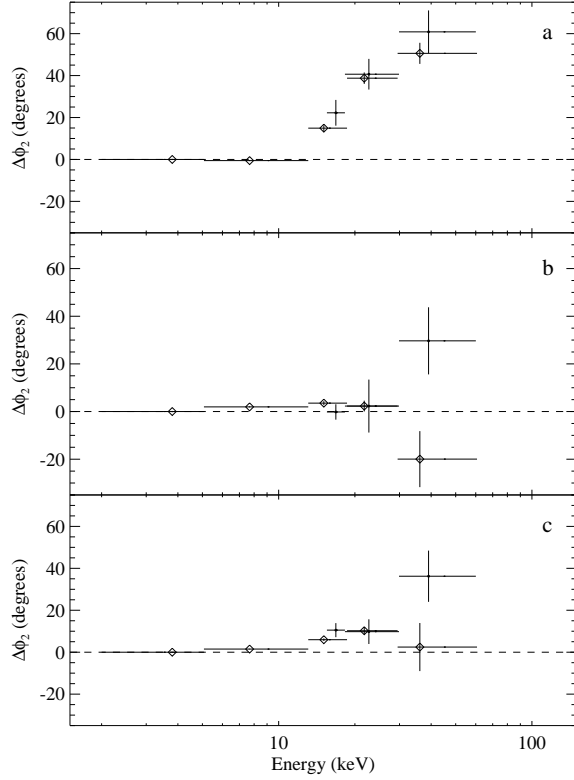


FIG. 11.— The phase lag for the first harmonic vs. energy relative to the 2-5 keV energy band (i.e.,  $\Delta\phi_2 = \phi_2(E) - \phi_2(2-5 \text{ keV})$ ) for orbits 1-3 (a), 4-6 (b) and 7-13 (c). The diamonds mark PCA measurements and the points mark HEXTE measurements.

#### REFERENCES

- Belloni, T. et al. 2000, *A&A* 355, 271  
 Böttcher, M. & Liang, E.P. 2000, astro-ph/0003139  
 Bradt, H.V., Rothschild, R.E. & Swank, J.H. 1993 *A&AS* 97, 355  
 Cui, W. 1999, *ApJ* 524, L59  
 Greiner, J., Morgan, E.H. & Remillard, R. 1996, *ApJ* 473, L107  
 Jackson, L.B. 1989, *Digital Filters and Signal Processing*, 2nd edition, Kluwer Academic Publishers  
 Lehr, D.E., Wagoner, R.V. & Wilms, J. 2000, astro-ph/0004211  
 Markwardt, C.B., Swank, J.H. & Taam, R.E. 1999, *ApJ* 513, L37  
 Mirabel, F. & Rodriguez, L. 1994, *Nature* 371, 46  
 Morgan, E.H., Remillard, R.A. & Greiner, J. 1997, *ApJ* 482, 993  
 Munro, M.P., Morgan, E.H. & Remillard, R.A. 1999, *ApJ* 527, 321  
 Nobili, L., Turolla, R., Zampieri, L. & Belloni, T. 2000, *ApJ* 538, L137  
 Reig, P. et al. 2000, astro-ph/0001134 v2  
 Sobczak, G.J. et al. 2000, astro-ph/0004215  
 Trudolyubov, S., Churazov, E. & Gilfanov, M. 1998, astro-ph/9811449  
 Wijnands, R., Homan, J. & van der Klis, M. 1999, *ApJ* 526, L33

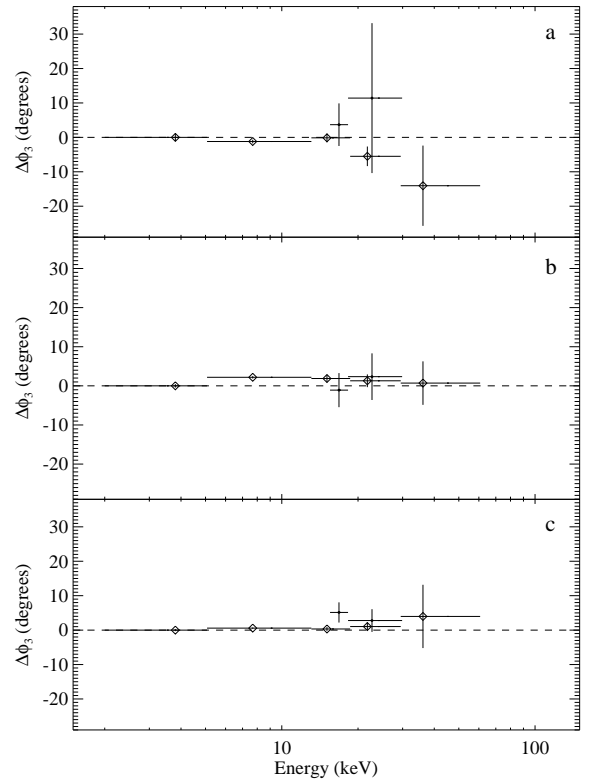


FIG. 12.— The phase lag for the second harmonic vs. energy relative to the 2-5 keV energy band (i.e.,  $\Delta\phi_3 = \phi_3(E) - \phi_3(2-5 \text{ keV})$ ) for orbits 1-3 (a), 4-6 (b) and 7-13 (c). The diamonds mark PCA measurements and the points mark HEXTE measurements.



TABLE 1  
GRS 1915+105 OBSERVATIONS FROM OCTOBER 1997

Orbit	MJD <sup>a</sup>	Exposure(s) <sup>b</sup>	QPO Frequency (Hz)	PCA Rate (cps) <sup>c</sup>	HEXTE Rate (cps) <sup>d</sup>
1	50729.347	3392	2.940	9349	62
2	50729.407	1599	2.627	8986	61
3	50730.414	3408	2.730	8815	60
4	50735.558	1960	0.844	7342	80
5	50737.421	2943	1.013	7338	75
6	50737.488	2158	1.064	7308	74
7	50743.301	1119	1.398	7319	70
8	50743.335	3161	1.358	7299	72
9	50743.416	2745	1.394	7262	70
10	50743.486	2377	1.437	7323	70
11	50746.553	2103	1.397	7334	71
12	50746.622	1975	1.481	7336	69
13	50746.692	1639	1.609	7432	68

<sup>a</sup>Modified Julian Date at the midpoint of the unocculted part of the orbit.

<sup>b</sup>On-source time for the PCA.

<sup>c</sup>2-30 keV count rate for 5 PCUs after background subtraction.

<sup>d</sup>15-124 keV HEXTE count rate after deadtime correction and background subtraction.

TABLE 2  
PHASE DIFFERENCES BETWEEN SINUSOIDAL COMPONENTS<sup>a</sup>

Orbits	$\phi_1 - \phi_2$	$\phi_1 - \phi_3$	$\phi_2 - \phi_3$
1-3	$256.27 \pm 0.32$	$256.75 \pm 1.10$	$0.48 \pm 1.13$
4-6	$226.49 \pm 0.32$	$232.58 \pm 0.49$	$6.08 \pm 0.53$
7-13	$239.00 \pm 0.20$	$242.23 \pm 0.32$	$3.23 \pm 0.35$

<sup>a</sup>The phase differences are for the 2-5 keV folded light curve and are given in degrees.